

PAPER • OPEN ACCESS

Characterization of cardiovascular and cerebrovascular controls via spectral causality analysis in patients undergoing surgical aortic valve replacement during a three-month follow-up

To cite this article: Vlasta Bari *et al* 2023 *Physiol. Meas.* **44** 094001

View the [article online](#) for updates and enhancements.

You may also like

- [A CT perfusion based model predicts outcome in wake-up stroke patients treated with recombinant tissue plasminogen activator](#)
Miloš Ajevi, Giovanni Furlanis, Alex Buoite Stella et al.
- [Functional magnetic particle imaging \(fMPI\) of cerebrovascular changes in the rat brain during hypercapnia](#)
Erica E Mason, Eli Mattingly, Konstantin Herb et al.
- [A non-invasive reference-based method for imaging the cerebral metabolic rate of oxygen by PET/MR: theory and error analysis](#)
Lucas Narciso, Tracy Ssali, Hidehiro Iida et al.



PAPER

OPEN ACCESS


RECEIVED
19 May 2023REVISED
22 August 2023ACCEPTED FOR PUBLICATION
13 September 2023PUBLISHED
29 September 2023

Original content from this work may be used under the terms of the [Creative Commons Attribution 4.0 licence](#).

Any further distribution of this work must maintain attribution to the author(s) and the title of the work, journal citation and DOI.



Characterization of cardiovascular and cerebrovascular controls via spectral causality analysis in patients undergoing surgical aortic valve replacement during a three-month follow-up

Vlasta Bari^{1,2,*}, Francesca Gelpi¹ , Beatrice Cairo¹, Martina Anguissola², Sara Pugliese², Beatrice De Maria³, Enrico Giuseppe Bertoldo⁴, Valentina Fiolo⁴, Edward Callus^{1,4}, Carlo De Vincentiis⁵, Marianna Volpe⁶, Raffaella Molfetta⁶, Marco Ranucci² and Alberto Porta^{1,2} 

¹ Department of Biomedical Sciences for Health, University of Milan, Milan, Italy

² Department of Cardiothoracic, Vascular Anesthesia and Intensive Care, IRCCS Policlinico San Donato, San Donato Milanese, Milan, Italy

³ IRCCS Istituti Clinici Scientifici Maugeri, Milan, Italy

⁴ Clinical Psychology Service, IRCCS Policlinico San Donato, San Donato Milanese, Milan, Italy

⁵ Department of Cardiac Surgery, IRCCS Policlinico San Donato, Milan, Italy

⁶ Department of Cardiac Rehabilitation, IRCCS Policlinico San Donato, Milan, Italy

* Author to whom any correspondence should be addressed.

E-mail: vlasta.bari@grupposandonato.it

Keywords: vector autoregressive model, causal squared coherence, baroreflex, cerebral autoregulation, aortic valve stenosis, surgical aortic valve replacement, heart rate variability

Abstract

Objective. Aortic valve stenosis (AVS) induces left ventricular function adaptations and surgical aortic valve replacement (SAVR) restores blood flow profile across aortic valve. Modifications of cardiac hemodynamics induced by AVS and SAVR might alter cardiovascular (CV) and cerebrovascular (CBV) controls. The study aims at characterizing CV and CBV regulations one day before SAVR (PRE), within one week after SAVR (POST), and after a three-month follow-up (POST3) in 73 AVS patients (age: 63.9 ± 12.9 yrs; 48 males, 25 females) from spontaneous fluctuations of heart period (HP), systolic arterial pressure, mean arterial pressure and mean cerebral blood velocity. **Approach.** CV and CBV regulations were typified via a bivariate autoregressive approach computing traditional frequency domain markers and causal squared coherence (CK^2) from CV and CBV variabilities. Univariate time and frequency domain indexes were calculated as well. Analyses were carried out in frequency bands typical of CV and CBV controls at supine rest and during active standing. A surrogate method was exploited to check uncoupling condition. **Main results.** We found that: (i) CV regulation is impaired in AVS patients; (ii) CV regulation worsens in POST; (iii) CV regulation recovers in POST3 and CV response to active standing is even better than in PRE; (iv) CBV regulation is preserved in AVS patients; (v) SAVR does not affect CBV control; (vi) parameters of the CBV control in POST3 and PRE are similar. **Significance.** CK^2 is particularly useful to characterize CV and CBV controls in AVS patients and to monitor of patient's evolution after SAVR.

1. Introduction

Stroke is an adverse event that might occur after surgical aortic valve replacement (SAVR) predominantly because of the formation of emboli during the surgical procedure (Daneault *et al* 2011). The overall rate of stroke after SAVR is between 2% and 4% depending on the patients' risk category (Kapadia *et al* 2018). The likelihood of developing stroke is time varying with higher values just after surgery (Kapadia *et al* 2018) and increasing during a follow-up of years (Messé *et al* 2014, Jørgensen *et al* 2021). The incidence of stroke raised up to 41%, if acute ischemic brain lesions are evaluated via brain diffusion-weighted magnetic resonance imaging (Altisent *et al* 2016), and to 54%, if silent stroke is considered (Grabert *et al* 2016).

Dynamic cerebral autoregulation (CA), namely the mechanism responsible for limiting mean cerebral blood flow (MCBF) variability in presence of modifications of mean arterial pressure (MAP) (Aaslid *et al* 1989, Paulson *et al* 1990), might play a protective role against cerebrovascular (CBV) adverse events after SAVR. If CA was impaired before surgery the resulting likelihood of developing stroke might be higher. Even if CA seems to be preserved before SAVR, as observed in small size cohorts (Porta *et al* 2020, Pedro *et al* 2023), the development of CBV adverse events might be favored by the postoperative depression of the cardiovascular (CV) control, especially of the baroreflex function (Bauernschmitt *et al* 2007, Retzlaff *et al* 2009, Porta *et al* 2020). Indeed, fluctuations of arterial pressure (AP), that are not buffered by the action of an active baroreflex through suitable changes of heart period (HP) (Taylor and Eckberg 1996, Patton *et al* 1996; Porta *et al* 2023a), might drive variations of MCBF in presence of a weak CA via the pressure-to-flow relationship (Panerai *et al* 1999, Tzeng *et al* 2014, Bari *et al* 2022a, Gelpi *et al* 2022). CV and CBV controls are routinely inferred from the analysis of spontaneous fluctuations of systolic AP (SAP) and HP and of MAP and MCBF approximated as mean cerebral blood velocity (MCBv) (Laude *et al* 2004, Claassen *et al* 2016). Remarkably, recent studies suggested that CV and CBV regulatory mechanisms are linked such a way that a less efficient CV control can be compensated by a more reactive CA and vice versa (Tzeng *et al* 2010, Gelpi *et al* 2021, Rosenberg *et al* 2022). Therefore, in patients after SAVR it might be important to monitor concomitantly parameters of the baroreflex and CA (Porta *et al* 2023b) to clarify the role of regulatory mechanisms in modulating the risk of CBV adverse events and favor the development of countermeasures and tailored pharmacological treatments (Porta *et al* 2020).

CA is commonly assessed in the frequency domain via cross-spectral analysis applied to spontaneous variations of MAP and MCBv (Zhang *et al* 1998a, Zhang *et al* 1998b, Zhang *et al* 2002, Meel-van den Abeelen *et al* 2014, Liu *et al* 2020), while the same tool has been applied to the spontaneous variability of HP and SAP to derive information about CV control mechanisms such as the baroreflex (Saul *et al* 1991, Cooke *et al* 1999, Faes *et al* 2004, Porta *et al* 2013, Bari *et al* 2019). Frequency bands have been standardized to facilitate comparison among studies and account for different physiological mechanisms (Laude *et al* 2004, Claassen *et al* 2016). Among cross-spectral markers indexes assessing the degree of HP-SAP and MCBv-MAP associations, such as squared coherence (K^2) markers, have been found very useful because they varied with pathology and/or states of the autonomic function (Giller 1990, Zhang *et al* 1998b, Zhang *et al* 2002, Ocon *et al* 2009, Hamner *et al* 2010, Hamner *et al* 2012, Moura-Tonello *et al* 2016, Porta *et al* 2016b, Milan-Mattos *et al* 2018, Clemson *et al* 2022).

One of the major weaknesses of cross-spectral markers in assessing the strength of the coupling between two time series y_1 on y_2 lies in its inability to describe directionality of the interactions (Porta and Faes 2016a). In other words, K^2 is high in presence of a strong open loop dependence of y_1 on y_2 , or of y_2 on y_1 , or a significant closed loop influence of y_1 on y_2 and vice versa. This makes K^2 a very unspecific index of association between two time series especially when they interact in closed loop and their degree of association might be different along the two arms of the closed loop such as in the case of HP-SAP and MCBv-MAP regulations. Indeed, HP and SAP interact in closed loop along the feedforward mechanical pathway and the baroreflex feedback (De Boer *et al* 1987, Saul *et al* 1991, Baselli *et al* 1994, Patton *et al* 1996, Porta *et al* 2002, Porta *et al* 2011, Bari *et al* 2018) and bidirectional influences are identified between MAP and MCBv along the pressure-to-flow and the flow-to-pressure pathways. The flow-to-pressure link is usually disregarded when modeling the dynamic MAP-MCBv interactions (Claassen *et al* 2016) and represents the Cushing-like reflexes that contribute to adjust the MAP in presence of situations of brain hypo/hyperperfusion (Cushing 1902, Bari *et al* 2017, McBryde *et al* 2017, Saleem *et al* 2018, Schmidt *et al* 2018, Vaini *et al* 2019, Bari *et al* 2021, Porta *et al* 2023b). Accounting for directionality of the interactions might be fundamental in SAVR population because the impairment of control mechanisms after SAVR, if present, could concern solely a specific temporal direction (i.e. from SAP to HP in the CV control and from MAP to MCBv in the CBV regulation) and induce adjustments of the directionality of the information flow that might be of different entity in the HP-SAP and MCBv-MAP closed loops (Porta *et al* 2011, Bari *et al* 2017, Porta *et al* 2023b). In addition, since the post-surgery autonomic depression (Hogue *et al* 1994, Compostella *et al* 2015, Porta *et al* 2020) is expected to recede with time after surgery (Kuo *et al* 1999, Demirel *et al* 2002), SAVR is an interesting model of changeable influence of CV control on CBV regulation that might be useful to clarify CV and CBV dynamic interactions.

The aim of this work is to monitor CV and CBV dynamic interactions in patients with severe aortic valve stenosis (AVS) scheduled for SAVR at different time points before and after surgery. CV and CBV regulations were evaluated using traditional frequency domain markers, such as K^2 and transfer function gain (TFG), and causal K^2 (CK^2) to account for directionality of the interactions. Responses of the CV and CBV controls were evoked by a postural challenge, namely active standing (STAND) soliciting the baroreflex (Cooke *et al* 1999, Marchi *et al* 2016b, De Maria *et al* 2019) and cerebral artery vasoconstriction linked to the sympathetic activation (Grubb *et al* 1991, Zhang *et al* 1998b, Carey *et al* 2001, Gelpi *et al* 2022). Preliminary results were presented at 12th Conference of the European Study Group on Cardiovascular Oscillations (Bari *et al* 2022b) and at 21st Mediterranean Electrotechnical Conference (MELECON) (Bari *et al* 2022c).

Table 1. Clinical and demographic data of SAVR patients.

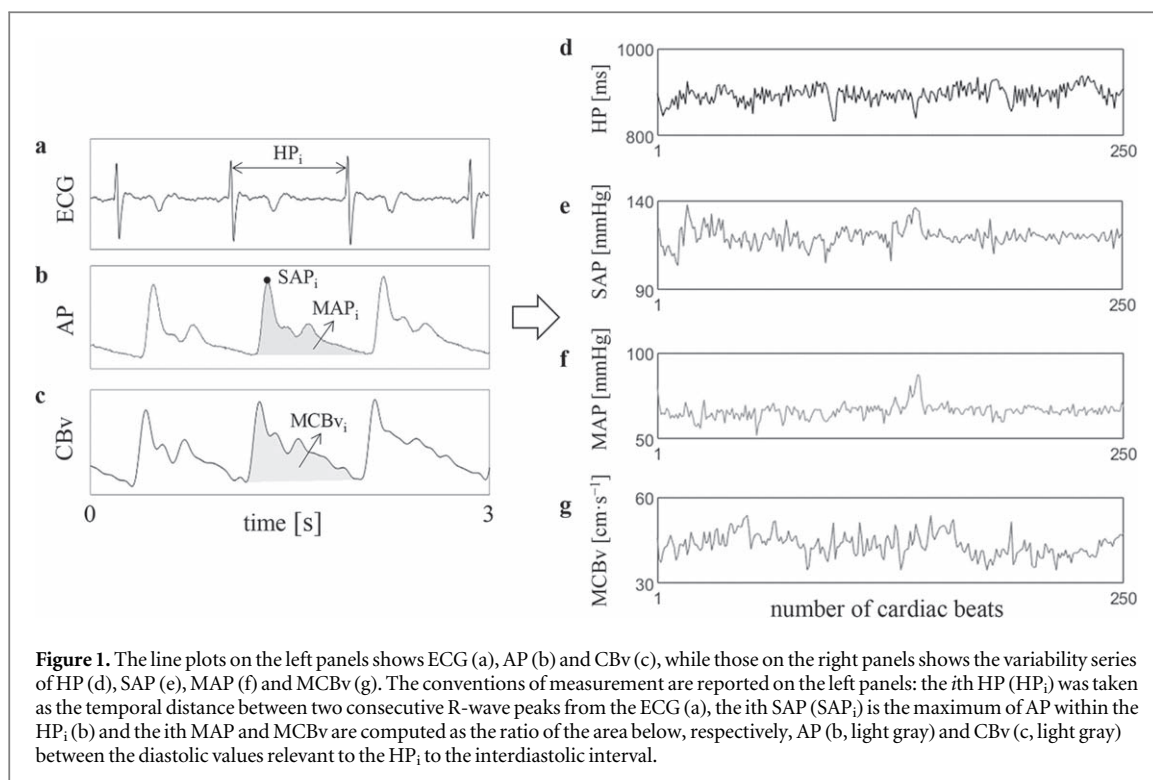
Parameter	SAVR (<i>n</i> = 73)
Age [years]	63.9 ± 12.9
Gender [male]	48 (66)
Weight [kg]	76.4 ± 14.5
BMI [kg·m ⁻²]	26.6 ± 11.2
AVS	73 (100)
Congestive heart failure	2 (3)
Recent myocardial infarction	0 (0)
Previous cerebrovascular events	0 (0)
LVEF [%]	59.1 ± 9.1
Diabetes	8 (11)
COPD	6 (9)
Serum creatinine [mg·dl ⁻¹]	0.95 ± 0.37
Hypertension	15 (21)
HCT [%]	41.2 ± 4.7
ACE inhibitors	18 (26)
Beta-blockers	26 (38)
Diuretics	16 (23)
Calcium antagonists	5 (7)
Antiarrhythmic drugs	3 (4)
Combined intervention	33 (47)
EuroSCORE II	2.2 ± 2.1
CPB time [minutes]	93.8 ± 41.8
Nadir temperature on CPB [°C]	38.2 ± 36.6
Catecholamine administration	9 (13)
Mechanical ventilation time [hours]	19.8 ± 62.7
ICU stay [days]	2.7 ± 8.9
Hospital stay [days]	9.2 ± 13.4
Postoperative atrial fibrillation	17 (24)
Postoperative arrhythmias	4 (6)
Postoperative low cardiac output syndrome	4 (6)
Postoperative stroke	0 (0)
Postoperative acute kidney injury	0 (0)
Hospital death	2 (3)

AVS = aortic valve stenosis; SAVR = surgical aortic valve replacement; BMI = body mass index; LVEF = left ventricular ejection fraction; COPD = chronic obstructive pulmonary disease; HCT = hematocrit; ACE = angiotensin converting enzyme; EuroSCORE = european system for cardiac operative risk evaluation; CPB = cardiopulmonary bypass; ICU = intensive care unit. Continuous data are presented as mean ± standard deviation and categorical data as number (percentage).

2. Experimental protocol and data analysis

2.1. Experimental protocol

Seventy-three subjects with severe AVS and scheduled for SAVR (age: 63.9 ± 12.9 years; 48 males, 25 females) were enrolled at the Department of Cardiothoracic, Vascular Anesthesia and Intensive Care of IRCCS Policlinico San Donato, Milan, Italy. The study was conducted according to the principles of the Declaration of Helsinki for medical research involving humans. The study was approved by the ethical review board of San Raffaele Hospital, Milan, Italy (approval number: 68/int/2018; approval date: 05/04/2018) and authorized by the IRCCS Policlinico San Donato, San Donato Milanese, Milan, Italy (authorization date: 13/04/2018). All subjects signed an informed consent prior to participation. Demographics, clinical and surgical characteristics, and types of medication of our SAVR cohort are summarized in table 1. Inclusion criteria were age higher than 18 years, AVS with indication for SAVR, spontaneous sinus rhythm and absence of overt autonomic and neurologic diseases, while exclusion criteria were absence of spontaneous sinus rhythm, signs of syncope during STAND or inability to maintain STAND position during the recording session and pregnancy. We recorded electrocardiogram (ECG) from lead II (BioAmp FE132, ADInstruments, Australia), non-invasive finger AP by volume-clamp photoplethysmography (CNAP Monitor 500, CNSystems, Austria) and cerebral blood velocity



(CBv) via a transcranial Doppler (TCD) device (Multi-Dop X, DWL, San Juan Capistrano, CA, USA) using an analog-to-digital converter (PowerLab, ADInstruments, Australia). Sampling rate was 400 Hz. AP was measured noninvasively from the middle finger of the non-dominant hand. Signals were acquired during quiet resting in supine position (REST) and during STAND. REST and STAND sessions lasted 10 min and REST always preceded STAND. The subjects were not allowed to talk during the protocol. A 5 min period of stabilization was allowed after having instrumented the subject and before starting signal acquisition. Subjects were acquired one day before intervention (PRE), within one week after intervention (POST) and after a three-month follow-up (POST3). CV control was assessed in PRE in 68 subjects at REST and 67 individuals during STAND, in POST in 44 subjects at REST and 41 individuals during STAND, and in POST3 in 17 subjects at REST and 17 individuals during STAND. CBV control was evaluated in PRE in 37 subjects at REST and 33 individuals during STAND, and in POST in 31 subjects at REST and 25 individuals during STAND, and in POST3 in 11 subjects at REST and 10 individuals during STAND. The number of recordings was different between CV and CBV series due to the difficulty in acquiring TCD signals of good quality especially in older subjects with pathology (Couture *et al* 2017). Furthermore, due to physical and psychological post-surgery debilitation several patients refused to repeat the tests in POST, and another additional percentage refused to come back to the hospital for POST3. The small differences between the number of recordings acquired during REST and STAND were due to the deterioration of the signal-to-noise ratio during STAND or to the possible loss of the TCD signal with the change of posture.

2.2. Extraction of the beat-to-beat variability series

From the ECG we calculated the HP as the time distance between two consecutive R-wave peaks. SAP was derived as the maximum of the AP signal within the i th HP, where i is the progressive cardiac counter. The i th diastolic value was taken as the minimum of AP after the i th SAP. The occurrences of the $(i-1)$ th and i th DAP values were utilized to compute the definite integral over AP and CBv and the result was divided by interdiastolic interval to derive, respectively, the i th MAP and MCBv. The conventions of the measurement are exemplified in figures 1(a)–(c). Series were extracted during all the time phases (i.e. PRE, POST, and POST3) and experimental conditions (i.e. REST and STAND). An example of variability series of HP, SAP, MAP and MCBv taken from a representative subject at REST is shown in figures 1(d)–(g). Series were manually checked by visualizing on the computer screen the position of the fiducial points, waveform morphology and variability series. If isolated anomalies of the cardiac rhythm were found, an automatic correction procedure was applied leading to the best linear interpolation between the most adjacent corrected values. If anomalies were not isolated, the interpolation procedure was applied again leading to the substitution of all anomalous values with linearly interpolated values between manually selected extremes. Analysis of data collected during STAND started after 3 min from the onset of the STAND challenge. A 5 min period of stabilization was allowed after having instrumented the subject and

before starting signal acquisition A linear trend was subtracted from variability series before the application of any frequency domain tool. Stationarity of the mean and variance of the detrended sequences was checked to limit the impact of nonstationarities over conclusions of the study (Magagnin *et al* 2011). Sequences of 256 consecutive values were selected with the onset of the sequence chosen in a random position but after three minutes from the starting of the recording.

2.3. Univariate time and frequency domain characterization of CV and CBV variability series

Beat-to-beat variability series of HP, SAP, MAP and MCBv underwent traditional time domain analysis assessing their mean μ and variance σ^2 . Markers were labeled as μ_{HP} , σ_{HP}^2 , μ_{SAP} , σ_{SAP}^2 , μ_{MAP} , σ_{MAP}^2 , μ_{MCBv} , σ_{MCBv}^2 and expressed respectively in ms, ms^2 , mmHg, mmHg^2 , mmHg, mmHg^2 , $\text{cm}\cdot\text{s}^{-1}$, $\text{cm}^2\cdot\text{s}^{-2}$. Frequency domain analysis was carried out over linearly detrended series after fitting the data with an autoregressive (AR) model (Baselli *et al* 1997). Power spectral density was computed from the transfer function of the AR model and the variance of the white noise feeding the AR model. The coefficients of the AR model and the variance of the white noise were estimated via Levinson–Durbin recursion. The optimal model order was chosen in the range from 8 to 14 via the Akaike information criterion. Power spectral density was factorized into components using the residue theorem and the power of each spectral component was computed and associated to the central frequency of the component (Baselli *et al* 1997). The power of each component was attributed to a frequency band according to value of its central frequency. As to the CV regulation, the low frequency (LF) band ranged from 0.04 to 0.15 Hz and the high frequency (HF) band from 0.15 to 0.4 Hz (Task Force of the European Society of Cardiology and the North American Society of Pacing and Electrophysiology 1996). The power of the HP series in the HF band was taken as an index of vagal modulation directed to the sinus node, marked as HF_{HP} and expressed in ms^2 (Pomeranz *et al* 1985). The power of the SAP series in the LF band was taken as an index of sympathetic modulation directed to the vessels, marked as LF_{SAP} and expressed in mmHg^2 (Pagani *et al* 1997). As to the CBV regulation, the very low frequency (VLF) band ranged from 0.02 to 0.07 Hz, the LF band ranged from 0.07 to 0.15 Hz and HF band from 0.15 to 0.4 Hz (Vaini *et al* 2019), the latter slightly adjusted from (Claassen *et al* 2016) to account for the possible presence of slow breathing rates. We computed the spectral power of MAP and MCBv variability series in the VLF, LF and HF bands and these indexes were denoted as VLF_{MAP} , LF_{MAP} , HF_{MAP} , VLF_{MCBv} , LF_{MCBv} , HF_{MCBv} and expressed in, respectively, mmHg^2 , mmHg^2 , mmHg^2 , $\text{cm}^2\cdot\text{s}^{-2}$, $\text{cm}^2\cdot\text{s}^{-2}$ and $\text{cm}^2\cdot\text{s}^{-2}$.

2.4. Computation of traditional frequency domain bivariate markers and CK^2

Parametric approach based on the identification of a bivariate AR model was utilized to compute K^2 and CK^2 (Porta *et al* 2002, Porta *et al* 2023). In the bivariate AR model, the current sample of one signal is described as a linear combination of past samples of the same signal and past, and eventually present, samples of the other signal plus a value of a Gaussian white noise realization with zero mean and variance to be estimated as well as the constant coefficients weighting the past samples in the linear regressions. After identifying the coefficients of the bivariate AR model, the spectral density matrix was derived from the transfer function matrix and the covariance matrix of the bivariate white noise feeding the model (Porta *et al* 2002, Porta *et al* 2023). The spectral density matrix contained the power spectral densities of the two series on the main diagonal and the power cross-spectral densities (i.e. from one series to the other and vice versa) out of it. The power cross-spectral densities exhibited identical modulus. Noncausal traditional K^2 was calculated as the ratio between the squared modulus of the power cross-spectral density divided by the product of the two power spectral densities (Saul *et al* 1991). Noncausal TFG was computed as the ratio of the modulus of the power cross-spectral density to the power spectral density of the input series (Saul *et al* 1991). CK^2 was computed by leaving unvaried the coefficients of the cross-regression of one series on the other and by forcing to 0 the coefficients of the cross-regression linking the latter to the former (i.e. in the reverse temporal direction), thus virtually opening the closed loop (Porta *et al* 2002). Traditional least squares approach was used to identify the coefficients of the bivariate AR model and the covariance matrix of the white noise. Cholesky decomposition method was utilized to solve the least squares problem (Porta *et al* 2000). The model order was optimized in the range between 5 and 12 according to the Akaike information criterion for multivariate processes (Akaike 1974). The inferior and superior limits of the order of the bivariate AR model order were set below that of the univariate AR model utilized for spectral analysis because the bivariate AR model features a greater spectral resolution as a result of its closed loop structure (Porta *et al* 2002). TFG, K^2 and CK^2 were computed as a function of the frequency. When studying the CV regulation, the two series were HP and SAP variabilities, while, when studying the CBV regulation, the two series were MCBv and MAP. TFG was calculated by taking SAP and MAP as inputs and denoted as $\text{TFG}_{HP-SAP}(f)$ and $\text{TFG}_{MCBv-MAP}(f)$ respectively. The traditional versions of K^2 were denoted as $K_{SAP,HP}^2(f)$ and $K_{MAP,MCBv}^2(f)$, while the causal versions were $CK_{HP\rightarrow SAP}^2(f)$ from HP to SAP and $CK_{SAP\rightarrow HP}^2(f)$ from SAP to HP and $CK_{MCBv\rightarrow MAP}^2(f)$ from MCBv to MAP and $CK_{MAP\rightarrow MCBv}^2(f)$ from MAP to MCBv. TFG, K^2 and CK^2 functions

were always sampled at the maximum in the assigned frequency band. The noncausal indexes were labelled as $\text{TFG}_{\text{HP-SAP}}(\text{LF})$, $\text{TFG}_{\text{HP-SAP}}(\text{HF})$, $\text{TFG}_{\text{MCBv-MAP}}(\text{VLF})$, $\text{TFG}_{\text{MCBv-MAP}}(\text{LF})$, $\text{TFG}_{\text{MCBv-MAP}}(\text{HF})$, $K_{\text{HP,SAP}}^2(\text{LF})$, $K_{\text{HP,SAP}}^2(\text{HF})$, $K_{\text{MAP,MCBv}}^2(\text{VLF})$, $K_{\text{MAP,MCBv}}^2(\text{LF})$ and $K_{\text{MAP,MCBv}}^2(\text{HF})$, while the causal ones were marked as $\text{CK}_{\text{HP} \rightarrow \text{SAP}}^2(\text{LF})$, $\text{CK}_{\text{HP} \rightarrow \text{SAP}}^2(\text{HF})$, $\text{CK}_{\text{MCBv} \rightarrow \text{MAP}}^2(\text{VLF})$, $\text{CK}_{\text{MCBv} \rightarrow \text{MAP}}^2(\text{LF})$, and $\text{CK}_{\text{MCBv} \rightarrow \text{MAP}}^2(\text{HF})$ in one time direction, and $\text{CK}_{\text{SAP} \rightarrow \text{HP}}^2(\text{LF})$, $\text{CK}_{\text{SAP} \rightarrow \text{HP}}^2(\text{HF})$, $\text{CK}_{\text{MAP} \rightarrow \text{MCBv}}^2(\text{VLF})$, $\text{CK}_{\text{MAP} \rightarrow \text{MCBv}}^2(\text{LF})$, and $\text{CK}_{\text{MAP} \rightarrow \text{MCBv}}^2(\text{HF})$ in the reverse time direction.

2.5. Surrogate data analysis

We applied a surrogate data approach to reject the null hypothesis of uncoupling between two series in connection with the computation of K^2 and CK^2 markers (Porta and Faes 2016a). From each original couple of variability series, we generated one hundred surrogate pairs for any subject, experimental condition, and time point of the analysis. The surrogate series were built via an approach preserving the amplitude distribution and power spectral density of the original series, while phases were substituted with numbers drawn from a uniform distribution between 0 and 2π . The use of two independent random phase sequences assured the uncoupling between the two realizations at any frequency (Palus 1997). Iteratively-refined amplitude-adjusted Fourier transform-based method was exploited (Schreiber and Schmitz 1996). The method assures the perfect preservation of the amplitude distribution, while the power spectral density is the best estimation after 100 iterations. Fast Fourier transformation speeded up the construction of the surrogates. K^2 and CK^2 markers were computed over the original and surrogate pairs. The best model order estimated over the original pair in any subject, experimental condition and time point was maintained when analyzing the surrogates. Markers derived from surrogates were computed using the same strategy to sample K^2 and CK^2 as from the original pairs. The 95th percentile of the K^2 and CK^2 marker distributions over the surrogates was calculated. If the marker computed over the original series was above the 95th percentile of the distribution of the indexes derived from surrogates, the null hypothesis of uncoupling was rejected. The percentages of subjects featuring a rejection of the null hypothesis of uncoupling was monitored in each frequency band, experimental condition, and time point. The percentages computed over noncausal markers were denoted as $K_{\text{HP,SAP}}^2(\text{LF})\%$, $K_{\text{HP,SAP}}^2(\text{HF})\%$, $K_{\text{MAP,MCBv}}^2(\text{VLF})\%$, $K_{\text{MAP,MCBv}}^2(\text{LF})\%$, $K_{\text{MAP,MCBv}}^2(\text{HF})\%$, while those calculate over the causal indexes were marked as $\text{CK}_{\text{HP} \rightarrow \text{SAP}}^2(\text{LF})\%$, $\text{CK}_{\text{HP} \rightarrow \text{SAP}}^2(\text{HF})\%$, $\text{CK}_{\text{MCBv} \rightarrow \text{MAP}}^2(\text{VLF})\%$, $\text{CK}_{\text{MCBv} \rightarrow \text{MAP}}^2(\text{LF})\%$, and $\text{CK}_{\text{MCBv} \rightarrow \text{MAP}}^2(\text{HF})\%$ in one time direction, and $\text{CK}_{\text{SAP} \rightarrow \text{HP}}^2(\text{LF})\%$, $\text{CK}_{\text{SAP} \rightarrow \text{HP}}^2(\text{HF})\%$, $\text{CK}_{\text{MAP} \rightarrow \text{MCBv}}^2(\text{VLF})\%$, $\text{CK}_{\text{MAP} \rightarrow \text{MCBv}}^2(\text{LF})\%$, and $\text{CK}_{\text{MAP} \rightarrow \text{MCBv}}^2(\text{HF})\%$ in the reverse time direction.

2.6. Statistical analysis

The Shapiro–Wilk test was applied to check the normal distribution of the data. A two-way analysis of variance (Holm–Sidak test for multiple comparisons) was applied to noncausal and causal markers to check differences between experimental conditions (i.e. REST and STAND) given the time point (i.e. PRE, POST or POST3) and differences across time points given the experimental condition. If the hypothesis of normality of the distribution failed, Mann–Whitney rank sum was applied. The level of significance of each test was lowered according to the number of comparisons to account for the multiple comparison issue. The significant difference among the proportions of rejections of the null hypothesis of uncoupling was tested via χ^2 test. Even in this case the level of significance was corrected to account for to the number of comparisons. Statistical analysis was performed with a commercial statistical software (Sigmaplot v.14.0, Systat Software, San Jose, CA, USA). The level of statistical significance of all the tests was set to 0.05.

3. Results

Table 2 summarizes time and frequency domain parameters of the CV regulation as function of the experimental conditions (i.e. REST and STAND) and time points (i.e. PRE, POST and POST3). In POST and POST3 μ_{HP} was lower than PRE both at REST and during STAND. In all the time points μ_{HP} decreased in STAND compared to REST. In POST σ_{HP}^2 was lower than PRE both at REST and during STAND, but it recovered in POST3. σ_{SAP}^2 and LF_{SAP} increased during STAND compared to REST in POST3 being the values during STAND higher than those observed in PRE and POST in the same experimental condition. μ_{SAP} and HF_{HP} remained unvaried with experimental condition and time point. The optimal order of the AR model utilized for univariate spectral analysis of HP and SAP series did not vary across either experimental conditions or time points.

Table 3 lists time and frequency domain parameters of the CBV regulation across experimental conditions and time points. In POST μ_{MAP} raised during STAND compared to REST. In POST3 σ_{MAP}^2 and LF_{MAP} increased during STAND compared to REST resulting in values during STAND higher than those observed in PRE and POST in the same experimental condition. At REST HF_{MAP} raised during POST compared to PRE, while in POST3 it was smaller than in POST. In POST, STAND induced a decrease of HF_{MAP} compared to REST. All

Table 2. Time and frequency domain indexes of the CV control at REST and during STAND in PRE, POST and POST3.

Parameter	PRE		POST		POST3	
	REST (<i>n</i> = 68)	STAND (<i>n</i> = 67)	REST (<i>n</i> = 44)	STAND (<i>n</i> = 41)	REST (<i>n</i> = 17)	STAND (<i>n</i> = 17)
μ_{HP} [ms]	929.7 ± 132.7	818.9 ± 123.1*	766.0 ± 115.8#	705.3 ± 117.6*#	895.3 ± 117.7§	799.6 ± 117.5*§
σ_{HP}^2 [ms ²]	1164.1 ± 1472.6	956.9 ± 1290.7	314.4 ± 596.3#	303.1 ± 557.4#	1267.3 ± 2626.7§	1360.2 ± 2618.4§
HF _{HP} [ms ²]	260.5 ± 557.6	149.0 ± 366.9	63.6 ± 168.3	73.8 ± 225.7	379.1 ± 985.0	428.2 ± 1265.1
μ_{SAP} [mmHg]	139.0 ± 26.8	134.8 ± 28.0	128.7 ± 20.4	130.8 ± 23.4	137.1 ± 26.5	131.7 ± 25.6
σ_{SAP}^2 [mmHg ²]	28.9 ± 24.2	43.4 ± 36.5	28.1 ± 17.4	43.6 ± 36.0	32.2 ± 38.3	131.9 ± 296.3*#§
LF _{SAP} [mmHg ²]	3.5 ± 4.8	9.7 ± 16.4	3.9 ± 5.0	6.9 ± 11.6	4.9 ± 11.7	39.8 ± 109.7*#§

HP = heart period; μ_{HP} = HP mean; σ_{HP}^2 = HP variance; SAP = systolic arterial pressure; μ_{SAP} = SAP mean; σ_{SAP}^2 = SAP variance; LF = low frequency; HF = high frequency; HF_{HP} = power of the HP series in the HF band expressed in absolute units; LF_{SAP} = power of the SAP series in the LF band expressed in absolute units. Results are reported as mean ± standard deviation. The symbol * indicates $p < 0.05$ versus REST within the same time point; the symbols # and § indicate $p < 0.05$, respectively, versus PRE and versus POST within the same experimental condition.

Table 3. Time and frequency domain indexes of the CBV control at REST and during STAND in PRE, POST and POST3.

Parameter	PRE		POST		POST3	
	REST (n = 37)	STAND (n = 33)	REST (n = 31)	STAND (n = 25)	REST (n = 11)	STAND (n = 10)
μ_{MCBv} [cm•s ⁻¹]	60.1 ± 31.0	48.5 ± 23.7	61.8 ± 32.7	56.0 ± 30.4	50.0 ± 19.1	46.1 ± 17.8
σ_{MCBv}^2 [cm ² •s ⁻²]	58.7 ± 104.9	43.0 ± 75.6	39.2 ± 44.2	37.2 ± 32.5	19.9 ± 21.4	65.1 ± 61.1
μ_{MAP} [mmHg]	97.1 ± 10.8	93.6 ± 16.0	87.5 ± 16.0	97.1 ± 19.0*	94.1 ± 19.7	98.2 ± 23.7
σ_{MAP}^2 [mmHg ²]	16.3 ± 11.4	24.6 ± 17.9	15.6 ± 10.8	16.7 ± 7.6	13.1 ± 6.9	47.6 ± 53.7*#§
VLF _{MCBv} [cm ² •s ⁻²]	6.1 ± 15.9	6.0 ± 12.9	4.6 ± 7.3	6.7 ± 10.2	2.8 ± 4.5	6.6 ± 10.9
LF _{MCBv} [cm ² •s ⁻²]	7.9 ± 19.4	3.9 ± 7.4	4.5 ± 7.3	3.5 ± 6.7	2.2 ± 3.9	12.1 ± 19.3
HF _{MCBv} [cm ² •s ⁻²]	18.4 ± 41.4	11.6 ± 24.7	10.7 ± 13.8	9.4 ± 12.3	5.5 ± 7.9	9.8 ± 10.0
VLF _{MAP} [mmHg ²]	2.0 ± 4.2	3.1 ± 6.5	1.8 ± 4.9	1.5 ± 3.2	1.7 ± 3.1	4.9 ± 4.8
LF _{MAP} [mmHg ²]	2.4 ± 3.0	7.2 ± 11.1	1.0 ± 1.2	2.4 ± 4.1	1.4 ± 1.5	8.0 ± 10.8*#§
HF _{MAP} [mmHg ²]	2.7 ± 2.3	3.9 ± 3.4	6.4 ± 6.2#	4.0 ± 2.5*	1.7 ± 1.0§	4.7 ± 4.7

MCBv = mean cerebral blood velocity; μ_{MCBv} = MCBv mean; σ_{MCBv}^2 = MCBv variance; MAP = mean arterial pressure; μ_{MAP} = MAP mean; σ_{MAP}^2 = MAP variance; VLF = very low frequency; LF = low frequency; HF = high frequency; VLF_{MCBv} = power of the MCBv series in the VLF band expressed in absolute units; LF_{MCBv} = power of the MCBv series in the LF band expressed in absolute units; HF_{MCBv} = power of the MCBv series in the HF band expressed in absolute units; VLF_{MAP} = power of the MAP series in the VLF band expressed in absolute units; LF_{MAP} = power of the MAP series in the LF band expressed in absolute units; HF_{MAP} = power of the MAP series in the HF band expressed in absolute units; Results are reported as mean ± standard deviation. The symbol * indicates $p < 0.05$ versus REST within the same time point; the symbols # and § indicate $p < 0.05$, respectively, versus PRE and versus POST within the same experimental condition.

Table 4. TFG of the CV control at REST and during STAND in PRE, POST and POST3.

Parameter	PRE		POST		POST3	
	REST (n = 68)	STAND (n = 67)	REST (n = 44)	STAND (n = 41)	REST (n = 17)	STAND (n = 17)
TFG _{HP-SAP(LF)} [ms•mmHg ⁻¹]	4.61 ± 2.98	3.31 ± 2.50	1.51 ± 1.27#	1.30 ± 1.15#	4.62 ± 5.01§	2.77 ± 2.20*
TFG _{HP-SAP(HF)} [ms•mmHg ⁻¹]	5.89 ± 5.68	4.85 ± 4.76	1.85 ± 1.72#	1.84 ± 2.63#	5.43 ± 5.44§	4.31 ± 4.81

TFG = transfer function gain; SAP = systolic arterial pressure; HP = heart period; LF = low frequency; HF = high frequency. Results are reported as mean ± standard deviation. The symbol * indicates $p < 0.05$ versus REST within the same time point; the symbols # and § indicate $p < 0.05$, respectively, versus PRE and versus POST within the same experimental condition.

MCBv parameters were unchanged regardless of time point and experimental condition. Again, the optimal model order utilized for univariate spectral analysis of MCBv and MAP series was similar across both experimental conditions and time points.

Table 4 summarizes the traditional TFG describing the CV regulation as a function of the experimental condition (i.e. REST and STAND) and time point (i.e. PRE, POST and POST3). The effect of STAND was significant solely in POST3 in the LF band. The impairment of CV control in POST compared to PRE and its recovery in POST3 compared to POST took the form, respectively, of the decrease and increase of both TFGs in the LF and HF bands at REST.

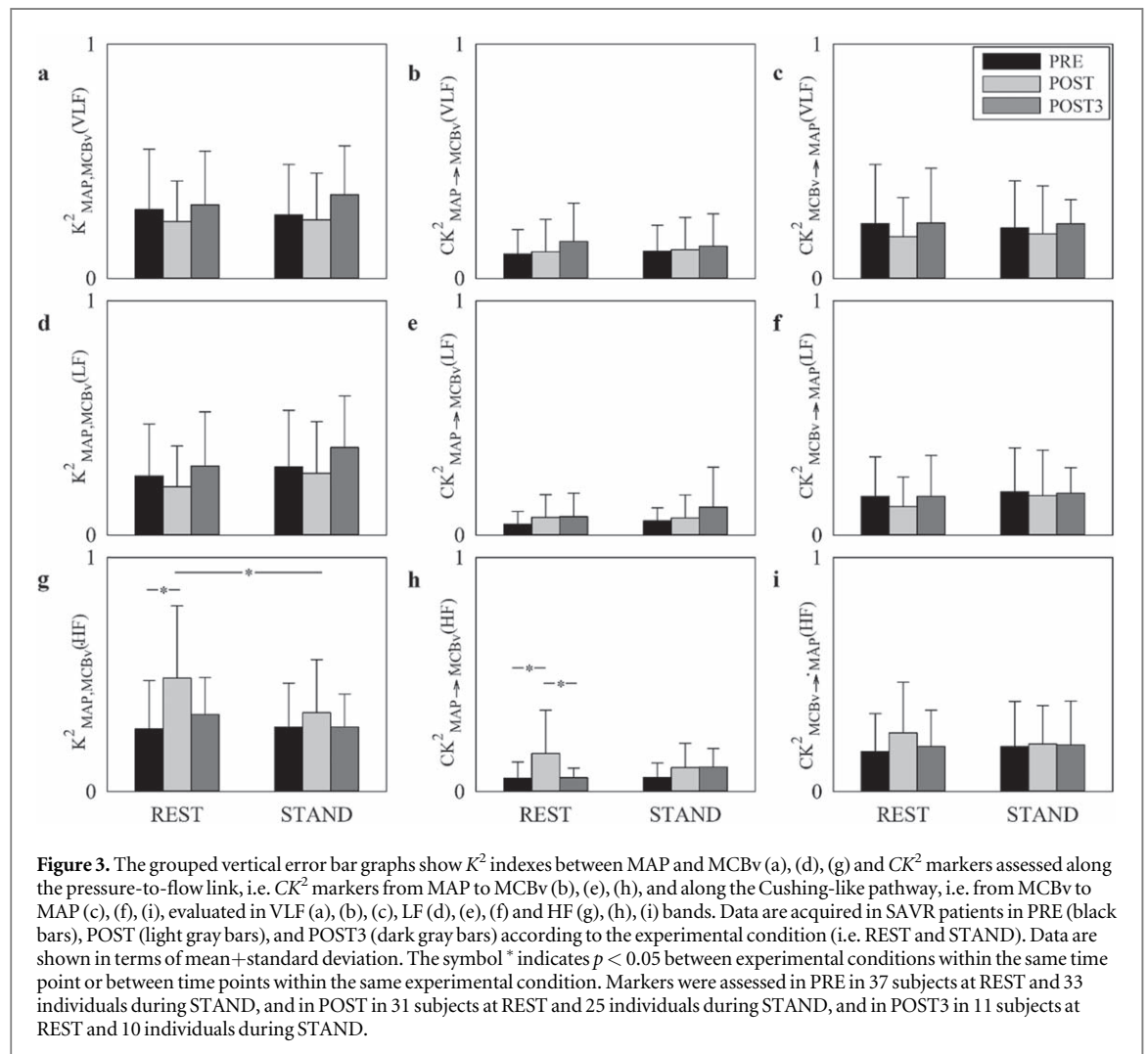
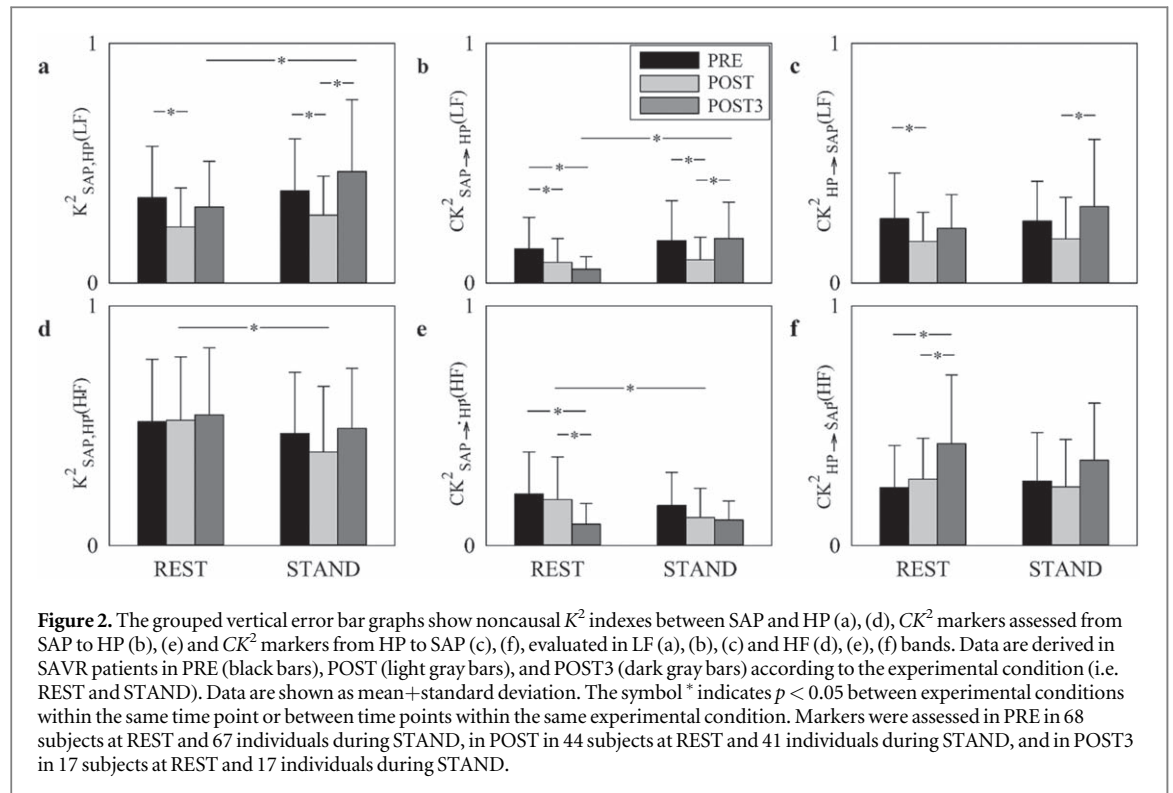
Table 5 lists the traditional TFG describing the CBV regulation as a function of the experimental condition (i.e. REST and STAND) and time point (i.e. PRE, POST and POST3). Regardless of the frequency band, no significant differences were detected across either experimental conditions or time points.

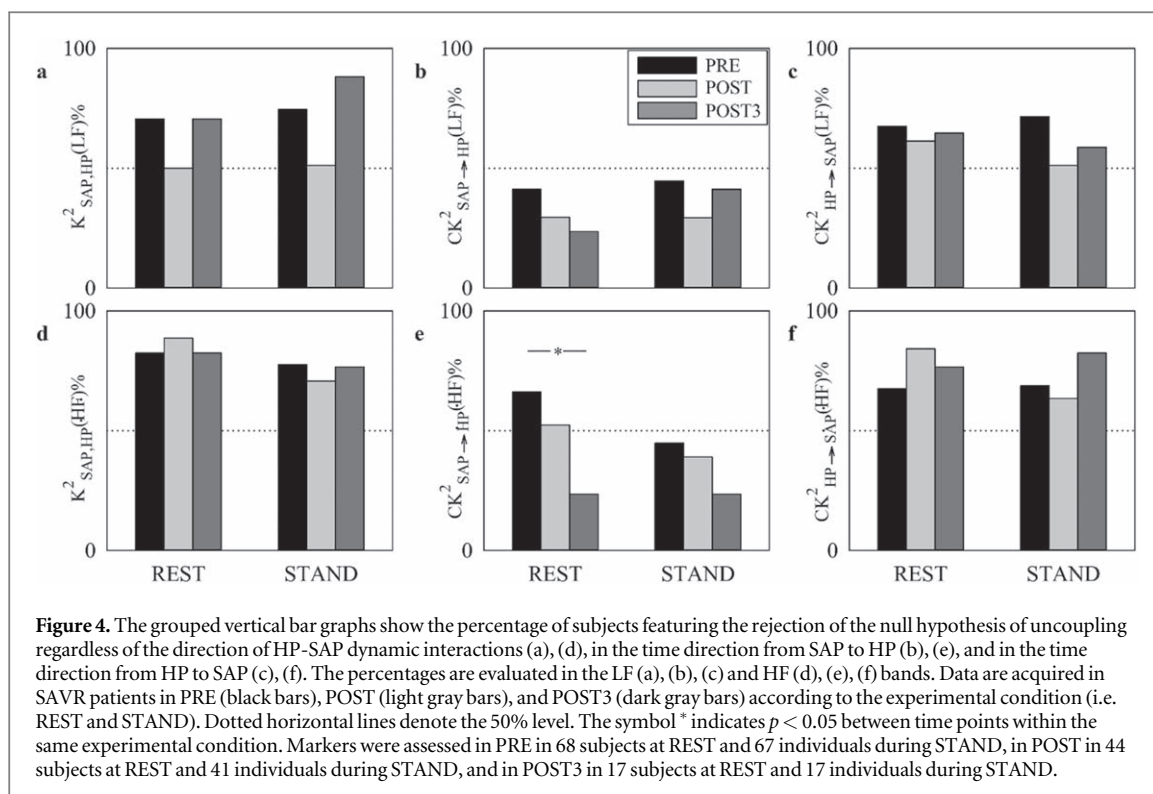
The grouped vertical bar graphs of figure 2 show noncausal markers between HP and SAP (figures 2(a), (d)), CK^2 indexes from SAP to HP (figures 2(b), (e)), and CK^2 indexes from HP to SAP (figures 2(c), (f)) assessed in LF (figures 2(a)–(c)) and HF (figures 2(d)–(f)) bands. Markers are reported as a function of the experimental condition (i.e. REST and STAND) in PRE (black bars), POST (light gray bars) and POST3 (dark gray bars). In the LF band, $K_{SAP,HP}^2(LF)$ was reduced in POST with respect to PRE at both REST and during STAND (figure 2(a)). In POST3 $K_{SAP,HP}^2(LF)$ was higher during STAND than at REST and during STAND $K_{SAP,HP}^2(LF)$ increased in POST3 compared to POST (figure 2(a)). On the baroreflex pathway at REST, $CK_{SAP \rightarrow HP}^2(LF)$ was smaller in POST and POST3 compared to PRE (figure 2(b)). In POST3 orthostatic challenge increased $CK_{SAP \rightarrow HP}^2(LF)$ compared to REST (figure 2(b)). During STAND, $CK_{SAP \rightarrow HP}^2(LF)$ was smaller in POST with respect to both PRE and POST3 (figure 2(b)). On the opposite arm, at REST $CK_{HP \rightarrow SAP}^2(LF)$ was lower in POST compared to PRE and during STAND $CK_{HP \rightarrow SAP}^2(LF)$ increased in POST3 with respect to POST (figure 2(c)). In the HF band

Table 5. TFG of the CBV control at REST and during STAND in PRE, POST and POST3.

Parameter	PRE		POST		POST3	
	REST (<i>n</i> = 37)	STAND (<i>n</i> = 33)	REST (<i>n</i> = 31)	STAND (<i>n</i> = 25)	REST (<i>n</i> = 11)	STAND (<i>n</i> = 10)
TFG _{MCBv-MAP} (VLF) [$\text{cm}\cdot\text{s}^{-1}\cdot\text{mmHg}^{-1}$]	0.83 ± 0.84	0.57 ± 0.36	0.88 ± 0.78	0.64 ± 0.35	0.64 ± 0.44	0.80 ± 0.51
TFG _{MCBv-MAP} (LF) [$\text{cm}\cdot\text{s}^{-1}\cdot\text{mmHg}^{-1}$]	0.79 ± 0.86	0.65 ± 0.38	0.66 ± 0.48	0.70 ± 0.37	0.70 ± 0.46	0.71 ± 0.22
TFG _{MCBv-MAP} (HF) [$\text{cm}\cdot\text{s}^{-1}\cdot\text{mmHg}^{-1}$]	1.22 ± 1.73	0.87 ± 0.56	0.88 ± 0.51	0.76 ± 0.41	0.81 ± 0.48	0.77 ± 0.49

TFG = transfer function gain; MAP = mean arterial pressure; MCBv = mean cerebral blood velocity; VLF = very low frequency; LF = low frequency; HF = high frequency. Results are reported as mean ± standard deviation.



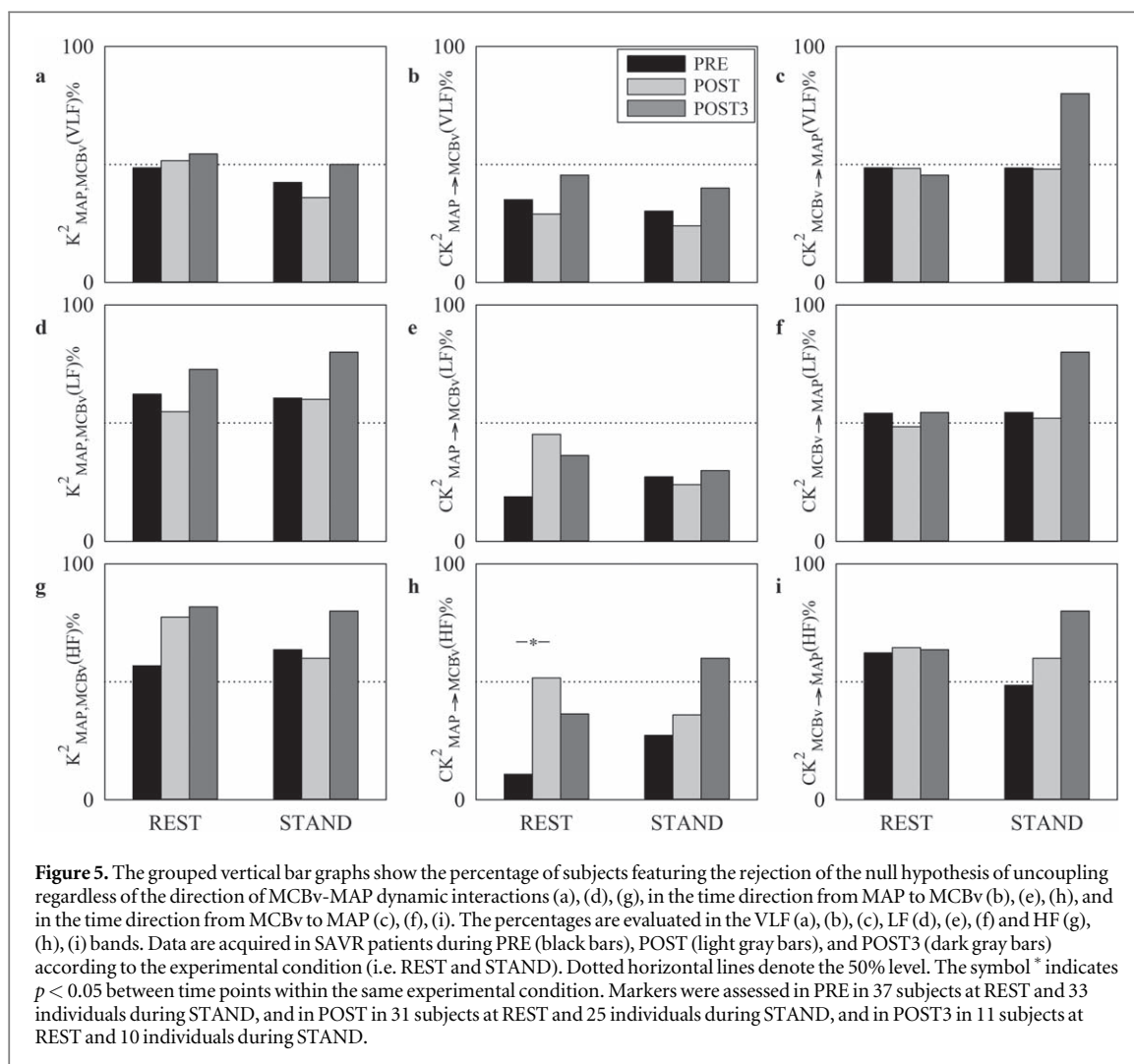


STAND reduced $K^2_{SAP,HP}(HF)$ in POST (figure 2(d)). At REST $CK^2_{SAP \rightarrow HP}(HF)$ was smaller in POST3 with respect to PRE and POST, and postural challenge decreased $CK^2_{SAP \rightarrow HP}(HF)$ in POST (figure 2(e)). At REST $CK^2_{HP \rightarrow SAP}(HF)$ increased in POST3 compared to PRE and POST (figure 2(f)). The optimal order of the AR model utilized for the bivariate analysis of the CV control did not vary across either experimental conditions or time points.

Figure 3 has the same structure as figure 2, but it shows the parameters describing the CBV regulation. Noncausal K^2 markers between MCBv and MAP are shown in figures 3(a), (d), (g), while CK^2 indexes from MAP to MCBv and from MCBv to MAP in figures 3(b), (e), (h), and figures 3(c), (f), (i) respectively. Markers are computed in the VLF (figures 3(a)–(c)), LF (figures 3(d)–(f)) and HF (figures 3(g)–(i)) bands. K^2 and CK^2 indices in the VLF (figures 3(a)–(c)) and LF (figures 3(d)–(f)) bands did not differ across either time points or experimental conditions. In the HF band, at REST $K^2_{MAP,MCBv}(HF)$ increased in POST compared to PRE and STAND reduced $K^2_{MAP,MCBv}(HF)$ in POST (figure 3(g)). At REST $CK^2_{MAP \rightarrow MCBv}(HF)$ was higher in POST with respect to PRE and POST3 (figure 3(h)), while $CK^2_{MCBv \rightarrow MAP}(HF)$ did not vary across either experimental conditions or time points (figure 3(i)). Again, the optimal model order utilized for the bivariate analysis of the CBV control was similar across experimental conditions and time points.

The grouped vertical bar graphs of figure 4 show the percentage of rejections of the null hypothesis of uncoupling regardless of the direction of HP-SAP dynamic interactions (figures 4(a), (d)), in the time direction from SAP to HP (figures 4(b), (e)), and in the time direction from HP to SAP (figures 4(c), (f)). The percentages are computed in the LF (figures 4(a)–(c)) and HF (figures 4(d)–(f)) bands and are reported as a function of the experimental condition (i.e. REST and STAND) in PRE (black bars), POST (light gray bars) and POST3 (dark gray bars). The percentage of subjects featuring the rejection of the null hypothesis of HP-SAP uncoupling remained unvaried with experimental condition and time point with the notable exception of $K^2_{SAP \rightarrow HP}(HF)$ % that at REST decreased in POST3 compared to PRE.

Figure 5 has the same structure as figure 4 but it shows the percentage of rejections of the null hypothesis of uncoupling regardless of the direction of MCBv-MAP dynamic interactions (figures 5(a), (d), (g)), in the time direction from MAP to MCBv (figures 5(b), (e), (h)), and in the time direction from MCBv to MAP (figures 5(c), (f), (i)). The percentages are computed in the VLF (figures 5(a)–(c)), LF (figures 5(d)–(f)) and HF (figures 5(g)–(i)) bands. No significant differences were found, and this conclusion held regardless of experimental condition and time point with the notable exception of $K^2_{MAP \rightarrow MCBv}(HF)$ % that at REST increased in POST compared to PRE.



4. Discussion

The main findings of this work can be summarized as follows: (i) the possibility to differentiate the pathways of a closed loop dynamic relationship provided by spectral causality analysis assures a more insightful description of CV and CBV controls; (ii) CV regulation is impaired in AVS patients; (iii) vagal control and CV regulation worsen in POST; (iv) CV regulation recovers in POST3 and its response to STAND is even better than in PRE; (v) CBV regulation is preserved in AVS patients; (vi) SAVR does not affect CBV control; (vii) parameters of the CBV control in POST3 are like those in PRE.

4.1. On the significance of using spectral causality analysis tools to assess CV and CBV regulations

Among the possible tools to assess spectral causality (Akaike 1968, Geweke 1982, Baccala and Sameshima 2001, Kaminski et al 2001, Porta et al 2002, Nollo et al 2005, Chen et al 2006, Chicharro 2011, Faes et al 2013a) in this study we exploited the CK^2 . This tool has the advantage of following directly from the definition of the traditional K^2 , thus directly checking the additional insight provided by CK^2 compared to K^2 analysis. Like any other spectral causality tool, CK^2 estimates the strength of the causal interaction in an assigned time direction in specific frequency bands that are deemed to be the most suitable for the evaluation of CV and CBV controls (Task Force of the European Society of Cardiology and the North American Society of Pacing and Electrophysiology 1996, Laude et al 2004, Claassen et al 2016). The relevance of using a spectral causality tool is evident from the difference of results derived from CK^2 along the two pathways and across frequency bands as well as from the comparison with K^2 indexes. For example, the percentage of rejections of the null hypothesis of uncoupling was higher in the time direction from HP to SAP and from MCBv to MAP than in the reverse causal directions, thus suggesting a more important impairment of the baroreflex control than the mechanical coupling between heart and vasculature in our population and a more significant tendency of CA to decouple MCBv and MAP along the pressure-to-flow link than the flow-to-pressure pathway. Therefore, the percentages of rejections of the null hypothesis of uncoupling, even when they are low, have a pathophysiological meaning. In addition,

HP-SAP spectral causal markers varied differently in LF and HF bands, thus stressing their specificity in describing diverse physiological mechanisms: for example, the increase of the strength of the casual relationship from SAP to HP during STAND compared to REST due to baroreflex activation induced by the postural challenge was detected only in the LF band, and the raise of the coupling strength from HP to SAP in POST3 compared to PRE, likely to be related to the improvement of cardiac mechanics, was detected only in the HF band. Peculiarities of CK^2 markers compared to noncausal bivariate frequency domain indexes are evident as well: for example, trends of CK^2 markers from SAP to HP with experimental condition and time point in the HF band were completely different from those of K^2 indexes and CK^2 markers were more powerful in separating experimental conditions and time points than TFG indexes.

4.2. CV regulation is impaired in AVS patients

Our cohort of patients underwent SAVR because of a severe AVS. The presence of a left ventricular outflow obstruction increased cardiac workload and led to left ventricle thickening and enlargement. This pathology is known to induce a chronic sympathetic activation driven by the need of maintaining cardiac output through the narrowed aortic valve (Dumonteil *et al* 2013). Sympathetic activation is known to affect baroreflex control by decreasing the baroreflex sensitivity (Cooke *et al* 1999, Marchi *et al* 2016b, De Maria *et al* 2019) and the high sympathetic driver at REST might contribute to the decoupling along the direction from SAP to HP (Nollo *et al* 2002, Milan-Mattos *et al* 2018). On the reverse pathway representing the mechanical link between heart and the vasculature, even though the incomplete diastolic runoff linked to the increased heart rate and peripheral vasoconstriction might contribute to the migration of the sensitivity of this pathway towards less negative values (Baselli *et al* 1994; Patton *et al* 1996, Porta *et al* 2013), the mechanical feedforward pathway is still working as proved by the preservation of the ejection fraction in our population. In agreement with these considerations in PRE at REST the percentage of rejections of the null hypothesis of the HP-SAP uncoupling along the mechanical feedforward pathway is significant, while the one along the baroreflex is below 50%. We expect that STAND reduces the HF_{HP} power and increases the LF_{SAP} one as a consequence of, respectively, the vagal withdrawal and sympathetic activation induced by the challenge (Pomeranz *et al* 1985, Montano *et al* 1994, Cooke *et al* 1999, Marchi *et al* 2016a), increases the degree of the HP-SAP association in the LF band (Porta *et al* 2016b, Bari *et al* 2017), especially along the baroreflex as a consequence of the baroreceptor unloading (Nollo *et al* 2005), and increases the percentage of rejections of the null hypothesis of the HP-SAP uncoupling along the baroreflex as a consequence of the increased strength along this time direction (Nollo *et al* 2005, Porta *et al* 2023b). These findings might be expected even in relation to the old age of our population, even though the impact of STAND might be reduced in ageing (Laitinen *et al* 1998). Since STAND did not produce these expected changes in our population, we conclude that autonomic function and baroreflex control are impaired in AVS population eligible for SAVR. This conclusion confirms preliminary observations of our group (Porta *et al* 2020). As a further sign of the CV regulation impairment, the expected decrease of the strength of the causal relationship from HP to SAP and the associated decrease of the percentage of rejections of the null hypothesis of the HP-SAP uncoupling in the LF band during STAND compared to REST was not detected (Nollo *et al* 2005, Porta *et al* 2023b). These findings indicate that a certain degree of impairment is present even along the mechanical feedforward pathway.

4.3. Vagal control and CV regulation worsen just after SAVR

SAVR worsens vagal control and CV regulation. The additional vagal withdrawal is suggested by the postoperative decrease of σ_{HP}^2 both at REST and during STAND. This result confirms previous observations made after cardiac surgery (Hogue *et al* 1994, Kuo *et al* 1999, Demirel *et al* 2002, Bauernschmitt *et al* 2007, Retzlaff *et al* 2009, Compostella *et al* 2015, Porta *et al* 2020). Since the postoperative depression of the vagal control summed up to a preoperative vagal impairment, this worsening might expose the patient to an additional risk of cardiac arrhythmias (Bauernschmitt *et al* 2007, Ranucci *et al* 2017), especially in relation to an unvaried sympathetic control as suggested by stable postoperative values of LF_{SAP} compared to PRE (Porta *et al* 2020). After surgery HP and SAP variability fluctuations were more independent, especially in the LF band (Porta *et al* 2020), as a sign of an additional deterioration of the CV regulation already present in PRE. As an original finding, the decrease of the strength of the HP-SAP dynamic interactions was the result of a significant decrement of both the coupling strength along the baroreflex and mechanical feedforward pathway. To further stress the dysfunction of the CV control STAND left unvaried the coupling strength along the baroreflex. These findings might suggest additional factors contributing to increase the risk of stroke just after SAVR (Daneault *et al* 2011, Altisent *et al* 2016, Grabert *et al* 2016) and to raise the likelihood of syncope during an orthostatic challenge just after SAVR (Jans and Kehlet 2017) because SAP variations are not buffered by suitable changes of HP. Remarkably, the likelihood of syncope increases after SAVR in presence of an improved cardiac hemodynamics.

4.4. CV regulation recovers three months after SAVR and its response to STAND is even better than in PRE

Time and frequency domain markers of HP and SAP variability suggest a recovery from the depression of vagal control as supported by the increase of σ_{HP}^2 in POST3 compared to POST observed both at REST and during STAND and a greater reactivity of the sympathetic control given that during POST3 the LF_{SAP} power raised significantly during STAND compared to REST. The recovery of heart rate variability indexes is in line with the well-known trends after major cardiac surgery (Demirel *et al* 2002). Since the LF_{SAP} power during STAND was larger in POST3 than in PRE, we can hypothesize that sympathetic control improved even compared to the baseline condition, as likely reflection of improved cardiac function reducing sympathetic overactivity at REST. However, the improvement did not involve vagal control directed to the heart because the HF_{HP} power did not vary. The trend toward the restoration of the CV control in POST3 took the form of the increase of the coupling strength between HP and SAP variability in the LF band compared to POST. This raise was evident during STAND, and it was significant both from HP to SAP and in the reverse time direction. These findings were not detected in the HF band, likely because the LF band covers the typical range of frequencies of the functioning of the baroreflex (Laude *et al* 2004) including the resonance frequency of the HP-SAP closed loop (De Boer *et al* 1987, Baselli *et al* 1994, Cevese *et al* 2001). The improvement of the CV regulation in POST3 was not only evident with respect to POST but also to PRE and the improvement involves both baroreflex and mechanical feedforward pathway. The amelioration of the baroreflex compared to PRE was suggested by the increase of the strength from SAP to HP in the LF band during STAND observed in POST3 but not visible in PRE, while the improvement of the mechanical feedforward pathway was indicated by the increase of the coupling strength from HP to SAP in the HF band during POST3 compared to PRE visible at REST.

4.5. CBV control is preserved in AVS patients

AVS reduces ventricular stroke volume and impairs the ability of the heart to modify cardiac output to cope with modifications of peripheral resistance (Carabello 2013). In heart failure patients secondary to myocardial infarction with reduced ejection fraction the MCBv is increased, and CA is impaired (Caldas *et al* 2017). It was proven that transcatheter aortic valve implantation improved cardiac output and cerebral blood flow in AVS patients (Vlastra *et al* 2021) and this result might suggest a cerebral hypoperfusion and a CA impairment before surgery. Conversely, CA is known to be preserved in AVS patients eligible for SAVR (Porta *et al* 2020, Pedro *et al* 2023). We confirm this finding by observing that at REST in PRE the strength of the MCBv-MAP dynamic relationship was limited especially in the time direction from MAP to MCBv and the percentage of the rejections of the null hypothesis of the MCBv-MAP uncoupling along the pressure-to-flow relationship was below 50% regardless of the frequency band, thus indicating that CA preserves its ability to limit the impact of MAP variability on MCBv changes (Zhang *et al* 2002, Bari *et al* 2017). The missed increase of the TFG of the MCBv-MAP relationship and of the strength of the MCBv-MAP association during STAND (Zhang *et al* 1998b, Zhang *et al* 2002, Bari *et al* 2017, Porta *et al* 2023b) corroborates the observation that CA is preserved. However, the limited impact of the orthostatic challenge on μ_{MCBv} and the negligible increase of MAP variability might have contributed to this conclusion. The conservation of the ejection fraction in our population might have impacted on the CA preservation as well (Caldas *et al* 2017). Remarkably, at REST in PRE the link along the flow-to-pressure relationship was significant in about 50% of the subjects, this fraction was maintained during STAND and this result held regardless of the frequency band, thus stressing the relevance of this pathway (Cushing 1902, Bari *et al* 2017, McBryde *et al* 2017, Saleem *et al* 2018, Schmidt *et al* 2018).

4.6. SAVR does not affect CBV control

We confirm that the CBV regulation was preserved just after SAVR (Porta *et al* 2020, Porta *et al* 2022, Pedro *et al* 2023). The original feature of this study is that this conclusion is based on spectral causality analysis. Indeed, the values of the degree of association between MCBv and MAP variability series were similar in PRE and POST and this finding did not depend on the direction of the interaction. Only in the HF band at REST we observed an increase of the coupling strength from MAP to MCBv in POST compared to PRE, likely owing to the increase of the HF_{MAP} power, but the HF_{MCBv} one remained unaltered and the percentage of subjects in which the null hypothesis of MCBv-MAP uncoupling was rejected remained about 50%, thus stressing the limited impact of MAP variations on MCBv changes. This conclusion is corroborated by stable values of the TFG of the MCBv-MAP relationship (Zhang *et al* 1998a, Zhang *et al* 2002). The conclusion about the CA preservation in POST appears to be robust because the orthostatic challenge was not able to affect the degree of the interaction from MAP to MCBv, while it is expected to increase in presence of CA dysfunction as it was observed in subjects prone to develop syncope while standing (Bari *et al* 2017, Porta *et al* 2023b). This conclusion might be related to the maintenance of a certain degree of sympathetic control in POST (Zhang *et al* 2002, Hamner *et al* 2010, Saleem *et al* 2018), while it indicates that vagal regulation is less involved in CA than previously suggested (Hamner *et al* 2012) given that the depression of the vagal control observed in POST has no impact on CA. Even the post-surgery

amelioration of the cardiac hemodynamics might have played a role in limiting the modifications of the MCBv-MAP relationship just after surgery. The coupling strength along the flow-to-pressure link was greater than that in the reverse causal direction, thus stressing the relevance of the Cushing-like reflex even during POST.

4.7. Three months after SAVR the CBV regulation is not significantly different from the one in PRE

In POST3 time and frequency domain analyses indicated that MCBv variability remained within ranges detected in PRE. Remarkably, in POST3 values of the TFG of the MCBv-MAP relationship were not modified even when the magnitude of MAP changes was increased in response to STAND. The strength of the coupling between MCBv and MAP variability series in POST3 was not significantly different from that in PRE and this result held regardless of the direction of interaction. In addition, STAND did not significantly influence the values of K^2 and CK^2 . This conclusion did not depend on the frequency bands. Remarkably, in the HF band in POST3 the coupling strength from MAP to MCBv, that was found to be increased in POST compared to PRE suggesting an impaired ability in buffering fast MAP changes with suitable modifications of cerebral resistances (Giller 1990, Zhang *et al* 1998b, Bari *et al* 2017), returned to values detected in PRE.

4.8. Limitations of the study, future developments, and clinical relevance of the approach

One of the main limitations of this work is due to the limited number of subjects acquired in the different experimental conditions, especially when the CBV control in POST3 phase was considered due to the difficulty in acquiring TCD signals in connection with that in recalling subjects at the follow-up. This fact has probably reduced the statistical power of the work, thus hampering the possibility to detect some differences. Furthermore, the present linear approach has a limited power in presence of nonlinearities of the involved physiological mechanisms and the possible nonlinear relationships among variables, thus suggesting the future use of model-free techniques to provide a more insightful description of nonlinear contributions to CV and CBV controls in AVS patients (Panerai *et al* 1999, Faes *et al* 2013b). However, the inherent nonlinear mechanisms underlying baroreflex and CA do not necessary produce evident nonlinear dynamics at the level of CV and CBV variabilities (Porta *et al* 2020) and this observation increases the relevance of linear analysis. Unfortunately, the study was not designed to evaluate sex differences. While enlarging the size of the group future studies should set it to ensure a sufficient statistical power to analyze the possible different behavior between males and females. The study suggests a methodological approach that can be applied in clinical settings to monitor individually the CV and CBV regulations and their postoperative evolution. Results indicate the need to favor a faster postoperative recovery of the CV control through the application of specific countermeasures and rehabilitation therapies. In addition, the invariance of the CBV control prompts for checking whether this conclusion could be confirmed even when considering specific AVS groups with reduced ejection fraction that might have exposed individuals to a chronic reduction of the brain perfusion.

5. Conclusion

This work proposes a spectral causality approach for the characterization of CV and CBV controls in AVS patients undergoing SAVR evaluated at different time points, namely just before SAVR, within one week after SAVR and after a three-month follow-up. CV and CBV mechanisms were challenged via an orthostatic challenge to evoke regulatory responses. The indexes suggested that the CV control was depressed in AVS patients, worsened just after SAVR and recovered after three months with CV responses to STAND even better than those observed before surgery. Conversely, the CBV regulation appears to be preserved in AVS patients and remained stable after surgery regardless of time point of the analysis. The proposed framework is particularly powerful because it allows the separation of the baroreflex from the mechanical feedforward pathway in the HP-SAP closed loop and the distinction of the pressure-to-flow relationship from the Cushing-like pathway in the MCBv-MAP closed loop. The framework assures the computation of highly specific CV and CBV markers compared to more traditional univariate and bivariate noncausal markers, thus increasing specificity of the analysis and the possibility to follow individual trends. In addition, results suggested that adverse events are more likely to be triggered by a deficit of the CV control, especially of the baroreflex function, more than linked to the CA dysfunction. This observation supports the use of specific countermeasures and pharmacological treatments aiming at limiting AP variations that might be not compensated by suitable adjustments of HP, especially in the period just after surgery. In addition to stress the resilience of the CBV control even in situations of vagal withdrawal such as in AVS patients before and after SAVR, this study emphasizes the role of the flow-to-pressure pathway even in situations of small variations of MAP and MCBv, thus suggesting the importance of Cushing-like reflexes in governing the degree of MCBv-MAP dynamic interaction, possible due to the preservation of the sympathetic control in the various phases of our experimental protocol. Given the recovery of the CV regulation is completed after three months and the improved cardiac function after SAVR, an additional improvement of the CV control might be expected after a

longer follow-up. This hypothesis deserves to be tested in future studies with a follow-up longer than three months. Lengthening the follow-up might be interesting even to check whether an improvement of the CV regulation could be associated to long-term modifications of the CBV control.

Data availability statement

The data cannot be made publicly available upon publication because they contain sensitive personal information. The data that support the findings of this study are available upon reasonable request from the authors.

Authors' contributions

Conceptualization: VB and AP; data curation: VB, FG, BC, MA, and SP; formal analysis: VB, FG, and BC; funding acquisition: MR and AP; investigation: VB, FG, BC, MA, SP, EGB, VF, EC, CDV, MV, RM, MR, and AP; methodology: AP; resources: VB, BC, EC, MR, and AP; software: AP; supervision: MR and AP; validation: VB and AP; visualization: VB and AP; writing—original draft: VB and AP; writing—review and editing: VB, FG, BC, MA, SP; BDM, EGB, VF, EC, CDV, MV, RM, MR, and AP.

Funding

The study was supported by the Italian Ministry of Health Grant RF-2016-02361069 to A Porta.

Conflict of interest

The authors declare that the research was conducted in the absence of any commercial or financial relationships that could be construed as a potential conflict of interest.

ORCID iDs

Francesca Gelpi  <https://orcid.org/0000-0002-9221-6153>

Alberto Porta  <https://orcid.org/0000-0002-6720-9824>

References

- Aaslid R, Lindegaard K F, Sorteberg W and Nornes H 1989 Cerebral autoregulation dynamics in humans *Stroke* **20** 45–52
- Akaike H 1968 On the use of a linear model for the identification of feedback systems *Ann. Inst. Stat. Math.* **20** 425–39
- Akaike H 1974 A new look at the statistical model identification *IEEE Trans. Autom. Control* **19** 716–23
- Altisent O A-J et al 2016 Neurological damage after transcatheter aortic valve implantation compared with surgical aortic valve replacement in intermediate risk patients *Clin. Res. Cardiol.* **105** 508–17
- Baccala L A and Sameshima K 2001 Partial directed coherence: a new concept in neural structure determination *Biol. Cybern.* **84** 463–74
- Bari V et al 2022a Exploring metrics for the characterization of the cerebral autoregulation during head-up tilt and propofol general anesthesia *Auton. Neurosci.: Basic Clin.* **242** 103011
- Bari V, De Maria B, Mazzucco C E, Rossato G, Tonon D, Nollo G, Faes L and Porta A 2017 Cerebrovascular and cardiovascular variability interactions investigated through conditional joint transfer entropy in subjects prone to postural syncope *Physiol. Meas.* **38** 976–91
- Bari V, Fantinato A, Vaini E, Gelpi F, Cairo B, De Maria B, Pistuddi V, Ranucci M and Porta A 2021 Impact of propofol general anesthesia on cardiovascular and cerebrovascular closed loop variability interactions *Biomed. Signal Process. Control* **68** 102735
- Bari V, Gelpi F, Cairo B, Cornara N, De Maria B, Ranucci M and Porta A 2022b Squared coherence analysis might suggest cerebral autoregulation post-surgery impairment in patients undergoing surgical aortic valve replacement *Proc. of the 12th Conf. of the European Study Group on Cardiovascular Oscillations (ESGCO)* (<https://doi.org/10.1109/ESGCO55423.2022.9931376>)
- Bari V et al 2022c An integrated multimodal approach to evaluate autonomic control, cerebral autoregulation and cognitive function in patients undergoing surgical aortic valve replacement during a 3-months follow-up *Proc. of the IEEE 21th Mediterranean Electrotechnical Conf. (MELECON)* pp 932–5
- Bari V, Ranucci M, De Maria B, Cairo B, Pistuddi V and Porta A 2018 Model-based directional analysis of cardiovascular variability identifies patients developing atrial fibrillation after coronary artery bypass grafting *Int. J. Cardiol.* **258** 97–102
- Bari V, Vaini E, Pistuddi V, Fantinato A, Cairo B, De Maria B, Dalla Vecchia L A, Ranucci M and Porta A 2019 Comparison of causal and non-causal strategies for the assessment of baroreflex sensitivity in predicting acute kidney dysfunction after coronary artery bypass grafting *Front. Physiol.* **10** 1319
- Baselli G, Cerutti S, Badilini F, Biancardi L, Porta A, Pagani M, Lombardi F, Rimoldi O, Furlan R and Malliani A 1994 Model for the assessment of heart period and arterial pressure variability interactions and respiratory influences *Med. Biol. Eng. Comput.* **32** 143–52
- Baselli G, Porta A, Rimoldi O, Pagani M and Cerutti S 1997 Spectral decomposition in multichannel recordings based on multivariate parametric identification *IEEE Trans. Biomed. Eng.* **44** 1092–101

- Bauernschmitt R, Malberg H, Wessel N, Brockmann G, Wildhirt S M, Kopp B, Kurths J, Bretthauer G and Lange R 2007 Autonomic control in patients experiencing atrial fibrillation after cardiac surgery *Pacing Clin. Electrophysiol.* **30** 77–84
- Caldas J R et al 2017 Cerebral blood flow autoregulation in ischemic heart failure *Am. J. Physiol.* **312** R108–13
- Carabelleo B A 2013 Introduction to aortic stenosis *Circ. Res.* **113** 179–85
- Carey B J, Manktelow B N, Panerai R B and Potter J F 2001 Cerebral autoregulatory responses to head-up tilt in normal subjects and patients with recurrent vasovagal syncope *Circulation* **104** 898–902
- Cevese A, Gulli G, Polati E, Gottin L and Grasso R 2001 Baroreflex and oscillation of heart period at 0.1 Hz studied by a-blockade and cross-spectral analysis in healthy humans *J. Physiol.* **531** 235–44
- Chen Y, Bressler S and Ding M 2006 Frequency decomposition of conditional Granger causality and application to multivariate neural field potential data *J. Neurosci. Methods* **150** 228–37
- Chicharro D 2011 On the spectral formulation of granger causality *Biol. Cybern.* **105** 331–47
- Claassen J A H R, Meel-van den Abeelen A S S, Simpson D M, Panerai R B and on behalf of the International Cerebral Autoregulation Research Network (CARNet) 2016 Transfer function analysis of dynamic cerebral autoregulation: a white paper from the International Cerebral Autoregulation Research Network *J. Cereb. Blood Flow Metab.* **36** 665–80
- Clemson P T, Hoag J B, Cooke W H, Eckberg D L and Stefanovska A 2022 Beyond the baroreflex: a new measure of autonomic regulation based on the time-frequency assessment of variability, phase coherence and couplings *Front. Netw. Physiol.* **2** 891604
- Compostella L, Russo N, Compostella C, Setzu T, D'Onofrio A, Isabella G, Tarantini G, Iliceto S, Gerosa G and Bellotto F 2015 Impact of type of intervention for aortic valve replacement on heart rate variability *Int. J. Cardiol.* **197** 11–5
- Cooke W H, Hoag J B, Crossman A A, Kuusela T A, Tahvanainen K U O and Eckberg D L 1999 Human responses to upright tilt: a window on central autonomic integration *J. Physiol.* **517** 617–28
- Couture E J, Desjardins G and Denault A Y 2017 Transcranial doppler monitoring guided by cranial two-dimensional ultrasonography *Can. J. Anaesth.* **64** 885–7
- Cushing H 1902 Some experimental and clinical observations concerning states of increased intracranial tension *Am. J. Med. Sci.* **124** 375–400
- Daneault B, Kirtane A J, Kodali S K, Williams M R, Genereux P, Reiss G R, Smith C R, Moses J W and Leon M B 2011 Stroke associated with surgical and transcatheter treatment of aortic stenosis a comprehensive review *J. Am. Coll. Cardiol.* **58** 2143–50
- De Boer R W, Karemaker J M and Strackee J 1987 Hemodynamic fluctuations and baroreflex sensitivity in humans: a beat-to-beat model *Am. J. Physiol.* **253** 680–9
- De Maria B, Bari V, Cairo B, Vaini E, Esler M, Lambert E, Baumert M, Cerutti S, Dalla Vecchia L and Porta A 2019 Characterization of the asymmetry of the cardiac and sympathetic arms of the baroreflex from spontaneous variability during incremental head-up tilt *Front. Physiol.* **10** 342
- Demirel S, Akkaya V, Oflaz H, Tükek T and Erk O 2002 Heart rate variability after coronary artery bypass graft surgery: a prospective 3 year follow-up study *Ann. Noninvasive Electrocardiol.* **7** 247–50
- Dumontel N et al 2013 Transcatheter aortic valve implantation reduces sympathetic activity and normalizes arterial spontaneous baroreflex in patients with aortic stenosis *JACC Cardiovasc. Interv.* **6** 1195–202
- Faes L, Porta A, Cucino R, Cerutti S, Antolini R and Nollo G 2004 Causal transfer function analysis to describe closed loop interactions between cardiovascular and cardiorespiratory variability signals *Biol. Cybern.* **90** 390–9
- Faes L, Erla S, Porta A and Nollo G 2013a A framework for assessing frequency domain causality in physiological time series with instantaneous effects *Phil. Trans. R. Soc. A* **371** 20110618
- Faes L, Porta A, Rossato G, Adami A, Tonon D, Corica A and Nollo G 2013b Investigating the mechanisms of cardiovascular and cerebrovascular regulation in orthostatic syncope through an information decomposition strategy *Auton. Neurosci.: Basic Clin.* **178** 76–82
- Gelpi F, Bari V, Cairo B, De Maria B, Tonon D, Rossato G, Faes L and Porta A 2022 Dynamic cerebrovascular autoregulation in patients prone to postural syncope: comparison of techniques assessing the autoregulation index from spontaneous variability series *Auton. Neurosci.: Basic Clin.* **237** 102920
- Gelpi F, Bari V, Cairo B, De Maria B, Tonon D, Rossato G, Faes L and Porta A 2021 Correlation between baroreflex sensitivity and cerebral autoregulation index in healthy subjects *Comput. Cardiol.* **48**
- Geweke J 1982 Measurement of linear dependence and feedback between multiple time series *J. Amer. Stat. Assoc.* **77** 304–13
- Giller C A 1990 The frequency-dependent behavior of cerebral autoregulation *Neurosurgery* **27** 362–8
- Grabert S, Lange R and Bleiziffer S 2016 Incidence and causes of silent and symptomatic stroke following surgical and transcatheter aortic valve replacement: a comprehensive review *Interact. Cardiovasc. Thorac. Surg.* **23** 469–76
- Grubb B P, Gerard G, Roush K, Temesy-Armos P, Montford P, Elliott L, Hahn H and Brewster P 1991 Cerebral vasoconstriction during head-upright tilt-induced vasovagal syncope: a paradoxical and unexpected response *Circulation* **84** 1157–64
- Hamner J W, Tan C O, Lee K, Cohen M A and Taylor J A 2010 Sympathetic control of the cerebral vasculature in humans *Stroke* **41** 102–9
- Hamner J W, Tan C O, Tzeng Y-C and Taylor J A 2012 Cholinergic control of the cerebral vasculature in humans *J. Physiol.* **590** 6343–52
- Hogue C W, Stein P K, Apostolidou I, Lappas D G and Kleiger R E 1994 Alterations in temporal patterns of heart rate variability after coronary artery bypass graft surgery *Anesthesiology* **81** 1356–64
- Jørgensen T H, Thyregod H G H, Ihlemann N, Nissen H, Petursson P, Kjeldsen B J, Steinbrüchel D A, Olsen P S and Søndergaard L 2021 Eight-year outcomes for patients with aortic valve stenosis at low surgical risk randomized to transcatheter vs. surgical aortic valve replacement *Eur. Heart J.* **42** 2912–9
- Kaminski M, Ding M, Truccolo W A and Bressler S 2001 Evaluating causal relations in neural systems: granger causality, directed transfer function and statistical assessment of significance *Biol. Cybern.* **85** 145–57
- Kapadia S R for the PARTNER Trial Investigators et al 2018 Stroke after surgical versus transfemoral transcatheter aortic valve replacement in the PARTNER trial *J. Am. Coll. Cardiol.* **72** 2415–26
- Kuo C-D, Chen G-Y, Lai S-T, Wang Y-Y, Shih C-C and Wang J-H 1999 Sequential changes in heart rate variability after coronary artery bypass grafting *Am. J. Cardiol.* **83** 776–9
- Jans Ø and Kehlet H 2017 Postoperative orthostatic intolerance: a common perioperative problem with few available solutions *Can. J. Anaesth.* **64** 10–5
- Laitinen T, Hartikainen J, Vanninen E, Niskamen L, Geelen G and Lansimies E 1998 Age and gender dependency of baroreflex sensitivity in healthy subjects *J. Appl. Physiol.* **84** 576–83
- Laude D et al 2004 Comparison of various techniques used to estimate spontaneous baroreflex sensitivity (the EuroBaVar study *Am. J. Physiol.* **286** R226–31

- Liu X, Czosnyka M, Donnelly J, Cardim D, Cabeleira M, Lalou D A, Hu X, Hutchinson P J and Smielewski P 2020 Assessment of cerebral autoregulation indices—a modelling perspective *Sci. Rep.* **10** 9600
- Magagnin V, Bassani T, Bari V, Turiel M, Maestri R, Pinna G D and Porta A 2011 Non-stationarities significantly distort short-term spectral, symbolic and entropy heart rate variability indices *Physiol. Meas.* **32** 1775–86
- Marchi A, Bari V, De Maria B, Esler M, Lambert E, Baumert M and Porta A 2016a Calibrated variability of muscle sympathetic nerve activity during graded head-up tilt in humans and its link with noradrenaline data and cardiovascular rhythms *Am. J. Physiol.* **310** R1134–43
- Marchi A, Bari V, De Maria B, Esler M, Lambert E, Baumert M and Porta A 2016b Simultaneous characterization of sympathetic and cardiac arms of the baroreflex through sequence techniques during incremental head-up tilt *Front. Physiol.* **7** 438
- McBryde F D, Malpas S C and Paton J F R 2017 Intracranial mechanisms for preserving brain blood flow in health and disease *Acta Physiol.* **219** 274–87
- Meel-van den Abeelen A S, van Beek A H, Slump C H, Panerai R B and Claassen J A 2014 Transfer function analysis for the assessment of cerebral autoregulation using spontaneous oscillations in blood pressure and cerebral blood flow *Med. Eng. Phys.* **36** 563–75
- Messé S R for the Determining Neurologic Outcomes from Valve Operations (DeNOVO) Investigators et al 2014 Stroke after aortic valve surgery Results from a prospective cohort *Circulation* **129** 2253–61
- Milan-Mattos J C, Porta A, Perseguini N M, Minatel V, Rehder-Santos P, Takahashi A C M, Mattiello S M and Catai A M 2018 Influence of age and gender on the phase and strength of the relation between heart period and systolic blood pressure spontaneous fluctuations *J. Appl. Physiol.* **124** 791–804
- Montano N, Gneccchi-Ruscione T, Porta A, Lombardi F, Pagani M and Malliani A 1994 Power spectrum analysis of heart rate variability to assess changes in sympatho-vagal balance during graded orthostatic tilt *Circulation* **90** 1826–31
- Moura-Tonello S C G, Porta A, Marchi A, Fagundes A A, Francisco C O, Rehder-Santos P, Milan-Mattos J C, Polaquini Simões R, Gois M O and Catai A M 2016 Cardiovascular variability analysis and baroreflex estimation in patients with type 2 diabetes in absence of any manifest neuropathy *PLoS One* **11** e0148903
- Nollo G, Faes L, Porta A, Antolini R and Ravelli F 2005 Exploring directionality in spontaneous heart period and systolic pressure variability interactions in humans: implications in the evaluation of baroreflex gain *Am. J. Physiol.* **288** H1777–85
- Nollo G, Faes L, Porta A, Pellegrini B, Ravelli F, Del Greco M, Disertori M and Antolini R 2002 Evidence of unbalanced regulatory mechanism of heart rate and systolic pressure after acute myocardial infarction *Am. J. Physiol.* **283** H1200–7
- Ocon A J, Kulesa J, Clarke D, Taneja I, Medow M S and Stewart J M 2009 Increased phase synchronization and decreased cerebral autoregulation during fainting in the young *Am. J. Physiol.* **297** H2084–95
- Pagani M, Montano N, Porta A, Malliani A, Abboud F M, Birkett C and Somers V K 1997 Relationship between spectral components of cardiovascular variabilities and direct measures of muscle sympathetic nerve activity in humans *Circulation* **95** 1441–8
- Palus M 1997 Detecting phase synchronisation in noisy systems *Phys. Lett. A* **235** 341–51
- Panerai R B, Dawson S L and Potter J F 1999 Linear and nonlinear analysis of human dynamic cerebral autoregulation *Am. J. Physiol.* **277** H1089–99
- Patton D J, Triedman J K, Perrott M H, Vidian A A and Saul J P 1996 Baroreflex gain: characterization using autoregressive moving average analysis *Am. J. Physiol.* **270** H1240–9
- Paulson O B, Strandgaard S and Edvinsson L 1990 Cerebral autoregulation *Cerebrovasc. Brain Metab. Rev.* **2** 161–92
- Pedro T, Costa A, Ferreira J, Rocha A L, Salgueiro E, Pereira G, Azevedo E and Castro P 2023 Changes in cerebral autoregulation and vasoreactivity after surgical aortic valve replacement: a prospective study *Exp. Physiol.* **108** 103–10
- Pomeranz B et al 1985 Assessment of autonomic function in humans by heart rate spectral analysis *Am. J. Physiol.* **248** H151–3
- Porta A, Bari V, Bassani T, Marchi A, Pistuddi V and Ranucci M 2013 Model-based causal closed-loop approach to the estimate of baroreflex sensitivity during propofol anesthesia in patients undergoing coronary artery bypass graft *J. Appl. Physiol.* **115** 1032–42
- Porta A, Baselli G, Rimoldi O, Malliani A and Pagani M 2000 Assessing baroreflex gain from spontaneous variability in conscious dogs: role of causality and respiration *Am. J. Physiol.* **279** H2558–67
- Porta A, Cairo B, Bari V, Gelpi F, De Maria B and Colombo R 2023 Model-based spectral causality of cardiovascular variability interactions during head-down tilt *Physiol. Meas.* **44** 054001
- Porta A, Catai A M, Takahashi A C M, Magagnin V, Bassani T, Tobaldini E, van de Borne P and Montano N 2011 Causal relationships between heart period and systolic arterial pressure during graded head-up tilt *Am. J. Physiol.* **300** R378–86
- Porta A and Faes L 2016a Wiener–Granger causality in network physiology with applications to cardiovascular control and neuroscience *Proc. IEEE* **104** 282–309
- Porta A et al 2020 Evaluation of the impact of surgical aortic valve replacement on short-term cardiovascular and cerebrovascular controls through spontaneous variability analysis *PLoS One* **15** e0243869
- Porta A, Furlan R, Rimoldi O, Pagani M, Malliani A and van de Borne P 2002 Quantifying the strength of the linear causal coupling in closed loop interacting cardiovascular variability signals *Biol. Cybern.* **86** 241–51
- Porta A et al 2022 Monitoring the evolution of asynchrony between mean arterial pressure and mean cerebral blood flow via cross-entropy methods *Entropy* **24** 80
- Porta A, Gelpi F, Bari V, Cairo B, De Maria B, Takahashi A C M, Catai A M and Colombo R 2023a Changes of the cardiac baroreflex bandwidth during postural challenges *Am. J. Physiol.* **324** R601–12
- Porta A, Gelpi F, Bari V, Cairo B, De Maria B, Tonon D, Rossato G and Faes L 2023b Concomitant evaluation of cardiovascular and cerebrovascular controls via Geweke spectral causality to assess the propensity to postural syncope *Med. Biol. Eng. Comput.* **online first in press**
- Porta A, Takahashi A C M and Catai A M 2016b Cardiovascular coupling during graded postural challenge: comparison between linear tools and joint symbolic analysis *Braz. J. Phys. Ther.* **20** 461–70
- Ranucci M, Porta A, Bari V, Pistuddi V and La Rovere M T 2017 Baroreflex sensitivity and outcomes following coronary surgery *PLoS One* **12** e0175008
- Retzlaff B, Bauernschmitt R, Malberg H, Brockmann G, Uhl C, Lange R, Kurths J, Bretthauer G and Wessel N 2009 Depression of cardiovascular autonomic function is more pronounced after mitral valve surgery: evidence for direct trauma *Phil. Trans. R. Soc. A* **367** 1251–63
- Rosenberg A J, Kay V L, Anderson G K, Luu M-L, Barnes H J, Sprick J D, Alvarado H B and Rickards C A 2022 The reciprocal relationship between cardiac baroreceptor sensitivity and cerebral autoregulation during simulated hemorrhage in humans *Auton. Neurosci.: Basic Clin.* **241** 103007
- Saleem S, Teal P D, Howe C A, Tymko M M, Ainslie P N and Tzeng Y C 2018 Is the Cushing mechanism a dynamic blood pressure-stabilizing system? Insights from Granger causality analysis of spontaneous blood pressure and cerebral blood flow *Am. J. Physiol.* **315** R484–95

- Saul J P, Berger R D, Albrecht P, Stein S P, Chen M H and Cohen R J 1991 Transfer function analysis of the circulation: unique insights into cardiovascular regulation *Am. J. Physiol.* **261** H1231–45
- Schmidt E A, Despas F, Pavy-Le Traon A, Czosnyka Z, Pickard J D, Rahmouni K, Pathak A and Senard J M 2018 Intracranial pressure is a determinant of sympathetic activity *Front. Physiol.* **9** 11
- Schreiber T and Schmitz A 1996 Improved surrogate data for nonlinearity tests *Phys. Rev. Lett.* **77** 635–8
- Task Force of the European Society of Cardiology and the North American Society of Pacing and Electrophysiology 1996 Heart rate variability: standards of measurement, physiological interpretation and clinical use *Circulation* **93** 1043–65
- Taylor J A and Eckberg D L 1996 Fundamental relations between short-term RR interval and arterial pressure oscillations in humans *Circulation* **93** 1527–32
- Tzeng Y-C, Lucas S J E, Atkinson G, Willie C K and Ainslie P N 2010 Fundamental relationships between arterial baroreflex sensitivity and dynamic cerebral autoregulation in humans *J. Appl. Physiol.* **108** 1162–8
- Tzeng Y C, MacRae B A, Ainslie P N and Chan G S H 2014 Fundamental relationships between blood pressure and cerebral blood flow in humans *J. Appl. Physiol.* **117** 1037–48
- Vaini E, Bari V, Fantinato A, Pistuddi V, Cairo B, De Maria B, Ranucci M and Porta A 2019 Causality analysis reveals the link between cerebrovascular control and acute kidney dysfunction after coronary artery bypass grafting *Physiol. Meas.* **40** 064006
- Vlastra W et al 2021 Cerebral blood flow in patients with severe aortic valve stenosis undergoing transcatheter aortic valve implantation *J. Am. Geriatr. Soc.* **69** 494–9
- Zhang R, Zuckerman J H, Giller C A and Levine B D 1998a Transfer function analysis of dynamic cerebral autoregulation in humans *Am. J. Physiol.* **274** H233–41
- Zhang R, Zuckerman J H and Levine B D 1998b Deterioration of cerebral autoregulation during orthostatic stress: insights from the frequency domain *J. Appl. Physiol.* **85** 1113–22
- Zhang R, Zuckerman J H, Iwasaki K, Wilson T E, Crandall C G and Levine B D 2002 Autonomic neural control of dynamic cerebral autoregulation in humans *Circulation* **106** 1814–20